

Letter

Zircon trace element constrains on the link between volcanism and plutonism in SE China

Li-Li Yan ^{a,b,1}, Zhen-Yu He ^{a,b,*}, Christoph Beier ^b, Reiner Klemm ^b^a Key Laboratory of Deep-Earth Dynamics, Institute of Geology, Chinese Academy of Geological Sciences, 26 Baiwanzhuang Road, Beijing 100037, China^b GeoZentrum Nordbayern, Friedrich-Alexander Universität Erlangen-Nürnberg, Schlossgarten 5, 91054 Erlangen, Germany

ARTICLE INFO

Article history:

Received 25 June 2018

Accepted 31 August 2018

Available online 5 September 2018

Keywords:

Zircon trace elements

Magma differentiation

Volcanic–plutonic connection

Yandangshan caldera complex

SE China

ABSTRACT

Trace elements in igneous zircon crystals are variable within single crystals or amongst populations of crystals and are particularly sensitive to changes in melt composition. In this study, we present zircon trace element data from both volcanic and plutonic rocks of the Yandangshan caldera complex from SEChina. The erupted rhyolitic rocks are interpreted to represent the most differentiated magma, whereas the intruded porphyritic quartz syenites are thought to be representative of the residual crystal mush. The zircon crystals of both lithologies are subdivided into two types based on their internal structures: type A with a distinct oscillatory growth zoning and type B crystals are bright in cathodoluminescence (CL-bright). Type B zircon occurs as rims of type A zircon or as individual grains. Compared to type A, type B zircons commonly show lower Hf, U, Th and Y concentrations and higher Ti and Zr/Hf and Eu/Eu* ratios. The zircon trace element compositions of the volcanic samples generally overlap those of the intracaldera porphyritic quartz syenite and mafic microgranular enclaves that contain both type A and type B zircons. Despite a general overlap, zircon grains from the volcanic rocks show relatively higher Hf contents and Y/Dy ratios, lower Ti contents and Th/U ratios and larger negative Eu anomalies than the plutonic samples. We suggest that the inter- and intragrain compositional variability of zircon crystals can be used to track the evolution of magmatic systems. We show that in our case, the volcanic and plutonic rocks crystallized continuously during the magmatic evolution in a common magma system and that the magmas of these rocks may be linked by fractional crystallization. Furthermore, the type B zircon grains are inferred to have crystallized in relatively hot and less evolved magma indicating a magma recharge event. Consequently, the geochemical variability of igneous zircon crystals can be used to infer on the magmatic evolution of single volcanic system which may also be applicable in other geodynamic environments.

© 2018 Elsevier B.V. All rights reserved.

1. Introduction

The relatively robust accessory mineral zircon is almost ubiquitous in highly silicic rocks and has high concentrations of certain trace elements, which make it a useful tool to track compositional changes of melts during magma evolution (e.g., Belousova et al., 2006; Claiborne et al., 2006; Hoskin and Schaltegger, 2003; Wark and Miller, 1993). The zircon trace element geochemistry has been widely used to identify magma-chamber processes in volcanic systems (e.g., Chamberlain et al., 2014; Cooper et al., 2014; Gagnevin et al., 2010; Klemetti et al., 2011; Reid et al., 2011; Schmitt et al., 2017; Storm et al., 2014), to evaluate the potential connection between high-silica volcanic units and coeval plutonic rocks (e.g., Barth et al., 2012; Buret et al., 2017; Claiborne et

al., 2006, 2010; Deering et al., 2016; Fohey-Breting et al., 2010) and to discriminate the tectonic setting of magmatism (Barth et al., 2013; Carley et al., 2014; Grimes et al., 2015).

Intensive Cretaceous volcanism and plutonism are widespread along the coastal area of SEChina, forming a larger scale, ca. 2000 km long volcanic–plutonic complex belt (Fig. 1a; Zhou et al., 2006). However, to date, the detailed assessment of the relationship between volcanic and plutonic rocks has only received little attention (He and Xu, 2012; Wang et al., 2000; Yan et al., 2016, 2018; Zhou et al., 2006). The Yandangshan caldera complex in this large-scale volcanic–plutonic complex belt is characterized by voluminous rhyolitic rocks associated with an intracaldera porphyritic quartz syenite (Fig. 1b; He et al., 2009; Yan et al., 2016). The ubiquity of zircon in the rock units of the Yandangshan caldera complex provides an excellent opportunity to evaluate the petrogenetic link between volcanic and shallow plutonic rocks in a single magmatic system from a mineral perspective. In this study, we present zircon trace element compositions obtained by laser ablation–inductively coupled plasma–mass spectrometry (LA-ICP-MS) for the rhyolitic volcanic rocks and porphyritic quartz syenite (and

* Corresponding author at: Institute of Geology, CAGS, 26 Baiwanzhuang Road, Beijing, China.

E-mail address: ahhzy@163.com (Z.-Y. He).

¹ Present address: School of Resources, Hebei GEO University, 136 Huai An Road, Shijiazhuang, 050031, China.

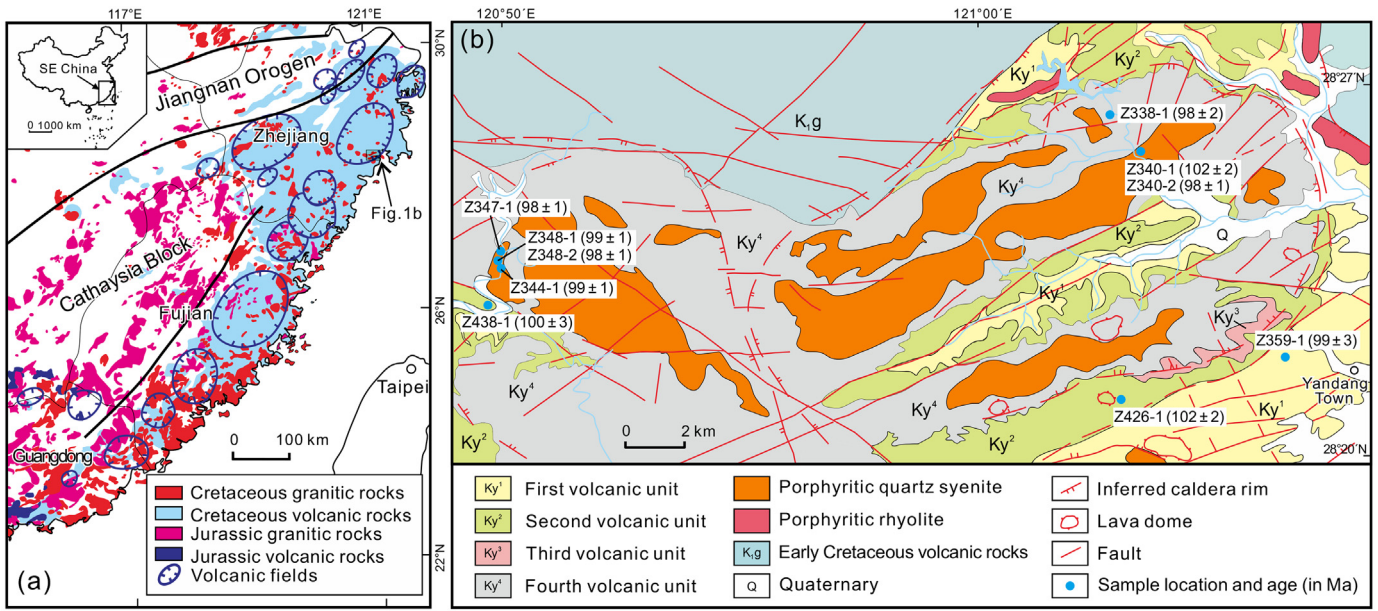


Fig. 1. (a) Simplified geological map of SE China showing the distributions of the Late Mesozoic granitic and volcanic rocks and the circular volcanic fields (modified after Zhou et al., 2006). (b) Geological sketch map of the Yandangshan caldera complex, showing the distribution of the volcanic and intracaldera plutonic rocks and sample localities and ages (modified from Yan et al., 2016).

mafic microgranular enclaves) of the Yandangshan caldera complex. The purpose of this research is: (1) to compare the zircon trace element geochemistry of the rhyolitic volcanic rocks with those obtained from the intracaldera porphyritic quartz syenite, and (2) to distinguish between magmatic processes, e.g., fractional crystallization, crystal accumulation and magma recharge using the texture and geochemistry of zircon grains. Our results indicate that the inter- and intragrain compositional variability of zircon crystals can be used to track the evolution of magmatic systems, and that zircon preserves an important mineral record for the extraction processes of silicic melt from crystal mushes (Bachmann and Bergantz, 2004).

2. Geological background

Intensive Cretaceous volcanism and plutonism in the coastal area of SE China was generated in an active continental margin environment which has generally been associated with the westward subduction of the paleo-Pacific plate (He and Xu, 2012; Jahn, 1974; Zhou et al., 2006). The volcanic products mainly consist of rhyolitic pyroclastic rocks and rhyolite lavas with a total outcrop area of ca. 90,000 km². They occur in several large volcanic fields containing calderas or caldera complexes intimately associated with shallow intracaldera plutons (Fig. 1a; Zhou et al., 2006; He et al., 2009; Yan et al., 2016, 2018).

The Yandangshan caldera (ca. 25 km in diameter) in the Zhejiang Province of SE China is composed of concentrically zoned volcanic units and several intracaldera porphyritic quartz syenite intrusions (Fig. 1b; He et al., 2009; Yan et al., 2016). The caldera forming volcanic units can be divided into four volcanic lithologies, representing four successive caldera-forming eruptions (Fig. 1b). The first and oldest volcanic unit comprises pyroclastic-flow deposits with a thickness of ~360 m. The rocks are dominantly rhyolitic welded crystal-lapilli tuffs with a well-developed eutaxitic texture. The second volcanic unit is approximately 500 m thick, and mainly consists of massive or flow-banded rhyolite with distinctive zones enriched in spherulites and lithophysae in some places. The third volcanic unit, about 380 m thick, is dominated by rhyolitic lapilli tuff and interlayered rhyolite. The fourth volcanic unit (the youngest unit) is dominated by rhyolitic welded crystal-vitric tuff with a thickness over 300 m showing a distinctive appearance of well-developed columnar jointing and eutaxitic texture. Darker pumice

clasts with ellipsoidal and banded form are locally observed. Porphyritic quartz syenites intruded in the center of the caldera and contain rare mafic microgranular enclaves with 5 to 15 cm in diameter. The mafic microgranular enclaves show subspherical to irregular shapes and are characterized by large plagioclase phenocrysts in a fine-grained groundmass (Supplementary Fig. 1). SHRIMP and LA-ICP-MS zircon U-Pb dating results revealed that the rhyolitic volcanic rocks and intracaldera porphyritic quartz syenite were emplaced contemporaneously within analytical errors (104 ± 2 – 98 ± 2 Ma; Fig. 1b; Supplementary Fig. 2; also see Yan et al., 2016).

The Yandangshan volcanic rocks are highly silicic, with SiO₂ contents of 69.6–71.6 wt% in the first unit, 73.1–76.3 wt% in the second unit, 70.1–74.9 wt% in the third unit, and 71.1–74.9 wt% in the fourth unit, broadly showing an increasing trend of SiO₂ contents. In comparison with the volcanic rocks, porphyritic quartz syenites have lower SiO₂ (65.0–66.1 wt%), thus showing a compositional gap (from about 66 to 70 wt% SiO₂) between the porphyritic quartz syenites and volcanic rocks (Yan et al., 2016).

3. Analytical methods

Zircon grains from 4 volcanic rock samples, 3 porphyritic quartz syenites and 3 mafic microgranular enclaves were analyzed for their trace element compositions. Cathodoluminescence (CL) images of the analyzed zircon grains were obtained using an FEI NOVA NanoSEM 450 scanning electron microscope equipped with a Gatan Mono CL4 cathodoluminescence system at the Institute of Geology, Chinese Academy of Geological Sciences.

Samples Z359-1, Z338-1, Z340-1 and Z340-2 were analyzed at the GeoZentrum Nordbayern, Friedrich-Alexander Universität Erlangen-Nürnberg, Germany, using a single collector quadrupole Agilent 7500i ICP-MS equipped with a 193 nm Analyte Excite laser ablation system (Teledyne Photon Machines). The glass reference material NIST SRM 612 was used as external standard for the silicates. BCR-2G was used to check the reproducibility and accuracy. The measurements were conducted using a spot size of 35 μm, 25 μm or 20 μm in diameter and a laser frequency of 20 Hz and ²⁹Si concentrations were used as internal standard. Detailed analytical procedures and data reduction procedures are listed in Günther et al. (2017). In-situ zircon trace element analyses

of the remaining samples were obtained simultaneously with the U-Pb dating using an Agilent 7500a ICP-MS equipped with a Coherent GeoLas Pro 193-nm laser ablation system in the State Key Laboratory of Mineral Deposits Research, Nanjing University. KL2-G was used to check the reproducibility and accuracy. Detailed analytical procedures are described by Yan et al. (2016). In this study, we convert Hf abundance into Zr/Hf using a stoichiometric Zr content of 500,000 ppm (Schmitt et al., 2017). The results of analyses of the international rock standards BCR-2G and KL2-G and the calculated analytical precision and accuracy are shown in Supplementary Table 1. The measured zircon trace element compositions and 1 sigma errors are provided in Supplementary Table 2.

4. Results

Based on the CL images, the zircon grains from 10 studied samples of the Yandangshan caldera complex were subdivided into two groups based on their internal structural domains (Fig. 2). The first type zircon (type A) has clear oscillatory growth zoning. The second type zircon (type B) is relatively CL-bright with generally weak zoning occurring either as the rim of the oscillatory zoned zircon (type A) or as individual zircon grain. We have previously demonstrated that the two zircon types have consistent ages and Hf-O isotope compositions, suggesting that they probably formed by a two-stage crystallization process from a single magmatic source (Supplementary Fig. 2; Yan et al., 2016). Plots of Hf versus Ti and Eu/Eu* versus Y/Dy, Zr/Hf and Sm/Yb ratios,

as well as Ti versus Yb and Th/U versus U, show distinct fields for the two zircon populations (Fig. 3). The type A zircon crystals have relatively high Hf (7147–15,625 ppm), U (36.0–366 ppm), Th (41.2–568 ppm) and Yb (123–838 ppm) and low Ti (5.51–37.5 ppm) contents and Eu/Eu* (0.19–0.55) ratios. Compared to type A zircon, type B zircon commonly shows lower Hf (5318–12,151 ppm), U (10.7–124 ppm), Th (18.5–313 ppm) and Yb (103–769 ppm), and higher Ti (12.1–49.8 ppm) contents and Zr/Hf (41.2–94.0) and Eu/Eu* (0.36–0.88) ratios (Supplementary Table 2; Figs. 3 and 4). It has to be noted, however that there are some overlaps and a few outliers within the two zircon groups (Figs. 3 and 4). For example, two analyses on type B zircon from the first volcanic unit have relatively low Eu/Eu* (0.15–0.30) ratios, while three analyses on type A zircon from the mafic microgranular enclaves show relatively high Eu/Eu* (0.57–0.69) ratios. Few type A zircons have relatively high Ti (26.2–37.5 ppm) contents. These are interpreted to reflect the presence of early nucleated zircons or the localized heterogeneous nucleation and growth (e.g., Reid et al., 2011).

Furthermore, zircon trace elements of the volcanic rocks overlap with those of the porphyritic quartz syenites and mafic microgranular enclaves (Figs. 3 and 4). The Hf compositions in zircon grains from the volcanic rocks (5318–13,673 ppm) overlap those of the porphyritic quartz syenites (6493–14,940 ppm) and mafic microgranular enclaves (6958–15,625 ppm). The Eu/Eu* values range from 0.15 to 0.73 for zircon grains from the volcanic rocks, 0.22 to 0.88 for zircon grains from the porphyritic quartz syenites and 0.19 to 0.88 for zircon grains from

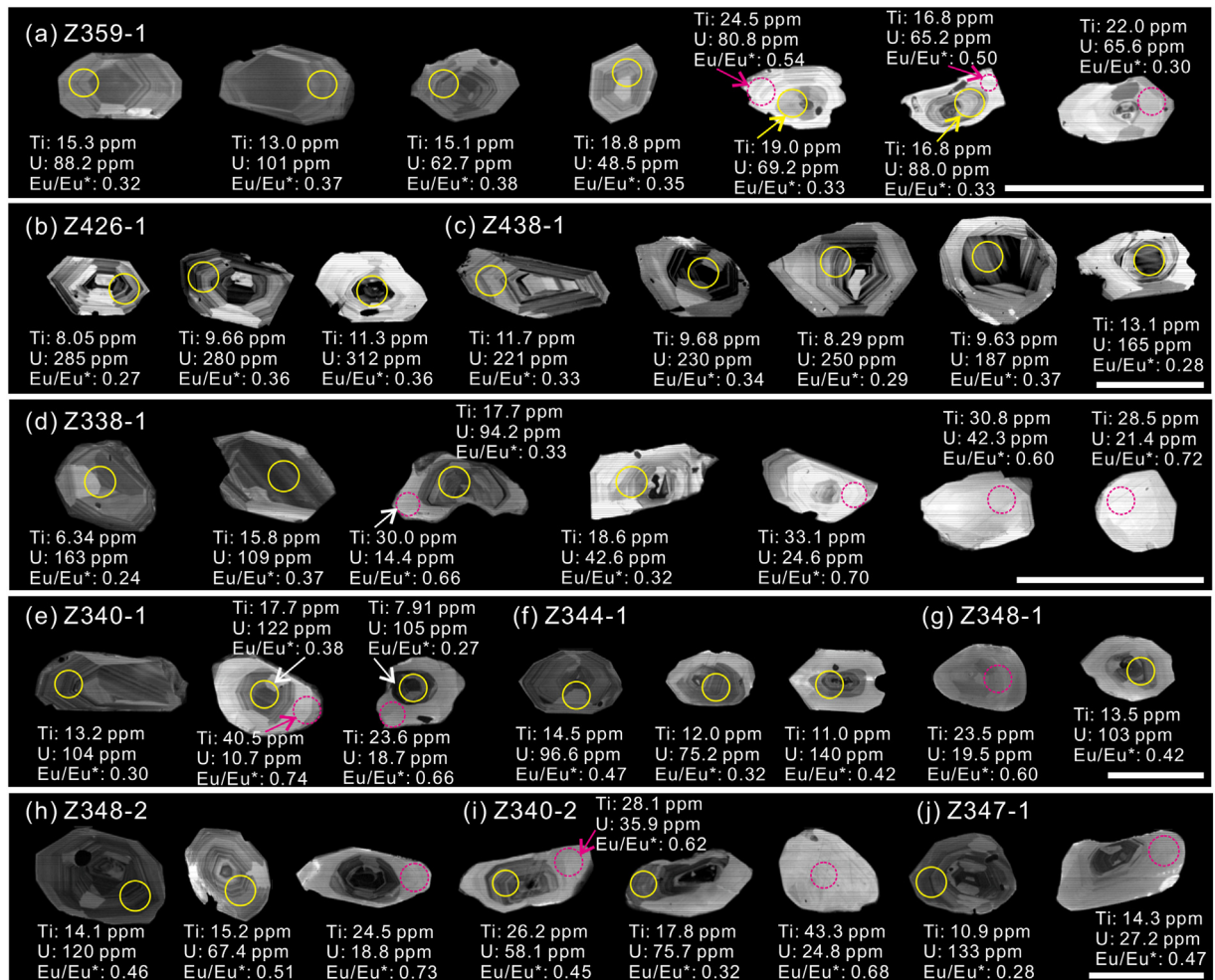


Fig. 2. CL images showing two types and corresponding trace element data of zircon in samples from the Yandangshan caldera complex. Yellow open circles indicate trace element analysis spots on type A zircon, and red dashed circles indicate analysis spots on type B zircon. (a) First volcanic unit. (b, c) Second volcanic unit. (d) Fourth volcanic unit. (e-g) Porphyritic quartz syenite. (h-j) Mafic microgranular enclave. Scale bars are 100 μ m.

the mafic microgranular enclaves (Figs. 3 and 4; Supplementary Table 2). In addition, zircons from the volcanic rocks have relatively high Y/Dy ratios (8.88–15.7), while those of the porphyritic quartz syenites and mafic microgranular enclaves are relatively low (7.58–13.3), although we note that they generally overlap (Figs. 3 and 4).

5. Discussion

5.1. Recharge of magma chamber revealed by multistage crystallization of zircon

The occurrence of two distinct zircon types in each of the rock units from the Yandangshan caldera complex requires a common process influencing both the volcanic and plutonic lithologies (Fig. 2). The type B zircon type zircons are relatively CL-bright with generally weak zoning,

however their high $(\text{Sm}/\text{La})_N$ (12–724) and Ce anomalies ($\text{Ce}/\text{Ce}^* = 10\text{--}94$) exclude late-stage hydrothermal formation (Supplementary Table 2; Hoskin and Schaltegger, 2003; Large et al., 2018). Furthermore, the type B and type A zircons show two chemically distinct zircon populations, ruling out the possibility that the type B zircons formed during a late-stage reheating event (Fig. 4; Bachmann and Bergantz, 2003; Buret et al., 2016). We propose here that the type B zircon was related to a magma recharge in a magma chamber system (e.g., Bachmann et al., 2002; Chamberlain et al., 2014; Claiborne et al., 2010; Large et al., 2018). The lower Hf, Yb and U and higher Ti, Zr/Hf and Eu/Eu* of the type B zircons is consistent with a hotter and less-evolved melt (Fig. 3; Claiborne et al., 2006, 2010; Ferry and Watson, 2007; Gagnevin et al., 2010; Reid et al., 2011; Barth et al., 2012; Cooper et al., 2014; Deering et al., 2016; Schmitt et al., 2017). The occurrence of a transgressive boundary between the type A zircon core and the type B zircon rim

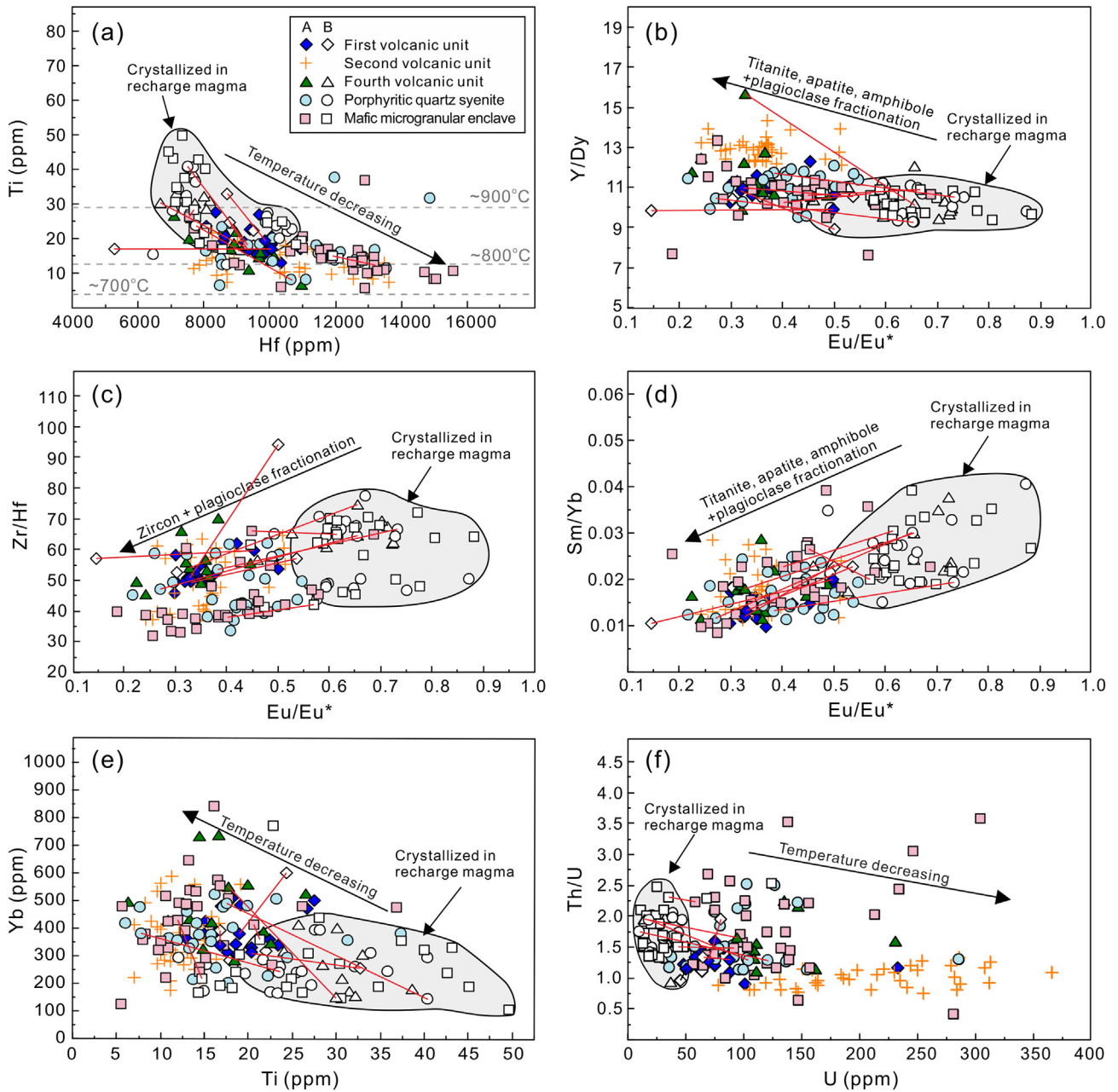


Fig. 3. Trace element compositional variations in zircon from samples of the Yandangshan caldera complex. A and B denotes type A and type B zircon respectively. Dashed lines in (a) represent estimated temperatures for a given Ti concentration, calculated from the Ti-in-zircon thermometer (Ferry and Watson, 2007) assuming $a_{\text{TiO}_2} = 0.75$ and $a_{\text{SiO}_2} = 1$. Representative tie-lines connect rim and core domains of single crystals. Labeled arrows suggest processes that could account for the observed covariations (after Gagnevin et al., 2010; Reid et al., 2011; Deering et al., 2016).

domains further suggests that the magma in which type A zircon grains had formed had subsequently been modified by magma recharge of the type B magma (Fig. 2). As a result type A crystals were partly resorbed and overgrown by type B zircon rims in the hotter and less-evolved recharge melts (e.g., Bachmann et al., 2002; Chamberlain et al., 2014; Claiborne et al., 2010; Gagnevin et al., 2010).

Magma recharge processes are often accompanied by the formation of mafic microgranular enclaves (e.g., Bachmann et al., 2002; Browne et al., 2006; Claiborne et al., 2010; Kennedy et al., 2016; Wright et al., 2011). In this study, type A and B zircon grains from the mafic microgranular enclaves in the porphyritic quartz syenite show the same internal textures and similar variation in trace element compositions compared to those from the volcanic samples and the host porphyritic quartz syenite (Figs. 2 and 3). This indicates that the type A zircons in the mafic microgranular enclaves had already formed when the recharge event occurred. Thus, the type A zircons were probably entrapped from the host magma during magma recharge. We suggest that the recharge magma is best represented by the mafic microgranular enclaves in the intracaldera porphyritic quartz syenite. The darker and finer-grained mafic microgranular enclaves are common in silicic plutonic and volcanic rocks, which have alternatively been proposed to be either residual source material (restite), hybrid magmas, cogenetic magmas (autoliths), or from unrelated magmas (Barbarin and Didier, 1992; Cantagrel et al., 1984; Kennedy et al., 2016; Perugini and Poli, 2012; Vernon, 1984; and references therein). Our case study here confirms that mafic microgranular enclaves in silicic plutons and volcanic rocks can be formed by injection of recharged cognate magmas

and must not necessarily indicate mixing of mafic mantle-derived and felsic crustal-derived magmas (e.g., Donaire et al., 2005; Shellnutt et al., 2010; Wright et al., 2011).

5.2. The volcanic-plutonic connection revealed by zircon trace elements

Zircon trace elements (such as Zr, Hf, Th, U, Y, Ti and REE) can be used to determine the conditions of crystallization and may record magmatic processes such as magma rejuvenation, magma mixing and fractional crystallization (Barth et al., 2012; Belousova et al., 2006; Chamberlain et al., 2014; Claiborne et al., 2006; Cooper et al., 2014; Hoskin and Schaltegger, 2003; Klemetti et al., 2011; Wark and Miller, 1993). Given the occurrence of zircon in the volcanic and plutonic rocks, we aim here to use the trace elements to decipher the processes influencing both rock types. For example, Hf in zircon commonly increases with decreasing temperature and increasing SiO₂ of the melt (Claiborne et al., 2006; Cooper et al., 2014; Reid et al., 2011). Plagioclase fractionation will deplete the residual melt in Eu²⁺ and zircon fractionation will remove Zr relative to Hf; hence the Eu/Eu* and Zr/Hf ratios will decrease with decreasing magmatic temperatures (Barth et al., 2012; Buret et al., 2016; Claiborne et al., 2006; Cooper et al., 2014; Deering et al., 2016; Reid et al., 2011; Schmitt et al., 2017). This is in agreement with decreasing Th/U ratios which also decrease as the magmas evolve (Barth et al., 2012; Buret et al., 2016; Chamberlain et al., 2014; Kemp et al., 2007; Kirkland et al., 2015).

As shown in Figs. 3 and 4, the trace elements of type A and type B zircons from all volcanic rocks and the porphyritic quartz syenites and

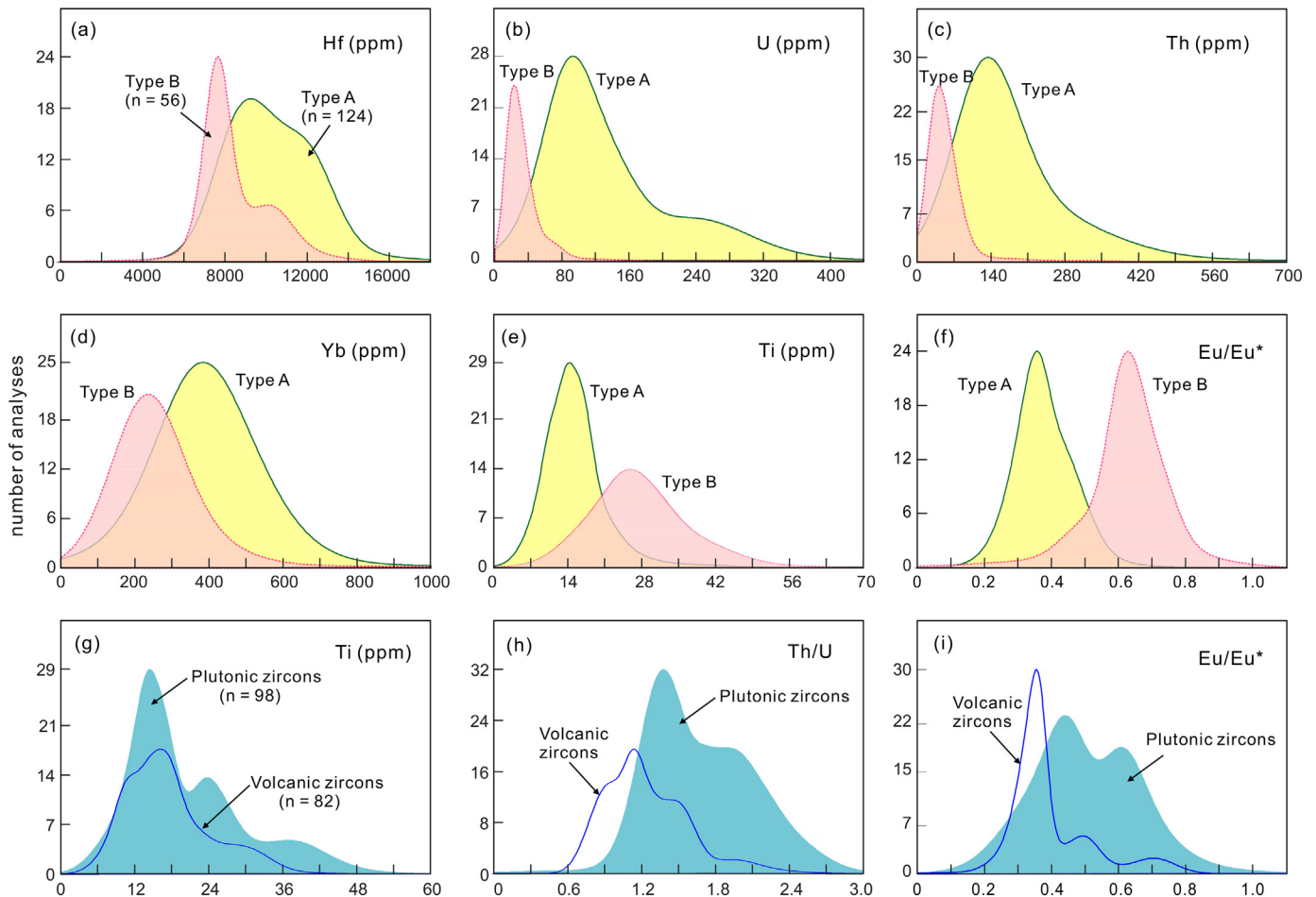


Fig. 4. Plots of Kernel density estimates showing the different trace element compositions of two distinct zircon types (a–f) and the overlaps between zircons from the volcanic and plutonic units (g–i) of the Yandangshan caldera complex.

mafic microgranular enclaves overlap, respectively. In particular, the trace elements of type A zircons display a broad correlation, indicating that Zr from the different rock units saturated almost contemporaneously and zircon crystallized continuously during the magmatic evolution (Fig. 3). Hafnium abundances in type A zircons increase with decreasing Ti, and the Y/Dy ratios increase with decreasing Eu/Eu*. The Sm/Yb and Zr/Hf ratios positively correlate with the Eu/Eu* ratios (Fig. 3). In addition, Yb and Ti show a very broad negative correlation for the type A zircons (Fig. 3), thereby suggesting that the magmas of these rocks are linked by fractional crystallization of amphibole, titanite, apatite, zircon and plagioclase (Fig. 3; Claiborne et al., 2006, 2010; Reid et al., 2011; Barth et al., 2012; Chamberlain et al., 2014; Deering et al., 2016). This is in agreement with abundant accessory titanite, apatite and zircon found in both volcanic and plutonic rocks of the Yandangshan caldera complex (Yan et al., 2016).

However, as mentioned above, a prominent silicic gap (from about 66 to 70 wt% SiO₂) exists between the volcanic rocks and porphyritic quartz syenite (Yan et al., 2016), which may be inconsistent with a continuous magma evolution. These disparities between the whole-rock and zircon compositions can be reconciled if the volcanic rocks represent the erupted melt expelled from a crystal-rich reservoir (crystal mush), which later crystallizes to form the plutonic rock assemblage (Bachmann and Bergantz, 2004; Cashman et al., 2017; Hildreth, 2004; Yan et al., 2016).

Zircon grains may be widely distributed due to the mobility of smaller zircon relative to the larger feldspar crystals that remain locked in crystal mush zones during liquid segregation events (Deering et al., 2011; Stelten et al., 2015). Therefore, zircon grains were continually mobilized by extracted melts or remained in the crystal mushes and thus recorded a continuous compositional range of magma evolution (e.g., Bachmann et al., 2002; Buret et al., 2016; Cooper and Kent, 2014; Wotzlaw et al., 2013). We note that although there are some overlaps between the zircon trace elements of the volcanic rocks and those of the porphyritic quartz syenite, the volcanic zircon grains, especially from the second unit, extend towards lower Ti contents and Th/U and Eu/Eu* ratios, and higher Hf contents and Y/Dy ratios (Figs. 3 and 4). This observation is consistent with the conclusion that the volcanic rocks represent highly evolved magmas, while the porphyritic quartz syenites represent the residual crystal mushes after the extraction of the rhyolite magmas (Yan et al., 2016, 2018).

6. Conclusions

- (1) Zircon trace element geochemistry shows that the Yandangshan volcanic rocks and the intracaldera porphyritic quartz syenite are linked by fractional crystallization in a common magma chamber system. The magmas of the volcanic rocks were extracted from crystal-rich reservoirs, while the porphyritic quartz syenite represents the residual crystal mushes.
- (2) Magma recharge processes were recorded in the zircon domains and some grains, which have lower Hf, Y and U, and higher Ti, Zr/Hf and Eu/Eu* relative to those of the zircon core domains, consistent with a formation from hotter and less-evolved melt. The recharge magma is represented by the mafic microgranular enclave in the intracaldera porphyritic quartz syenite, which confirms that mafic microgranular enclaves in silicic plutons and volcanic rocks can be formed by injection of recharged cognate magmas and do not necessarily indicate mixing of mafic mantle-derived and felsic crustal-derived magmas.
- (3) Zircon crystals may be used as indicators for the magmatic evolution of a single volcanic system and provide important constraints on the timescales and processes that influence active continental margin magmas. The preservation of zircon may thus provide a unique tool to infer on magmatic processes even in variably altered and old igneous systems.

Supplementary data to this article can be found online at <https://doi.org/10.1016/j.lithos.2018.08.040>.

Acknowledgments

We thank Prof. Nelson Eby, Yannick Buret and Rongfeng Ge for their constructive comments on the manuscript. We are grateful to Dr. H. Brätz for assistance with the LA-ICP-MS analysis. ChB thanks J. Henderson for help during the final revisions of this manuscript. This work was supported by the National Natural Science Foundation of China (41102028 and 41772060), and the Research Grant from Institute of Geology, CAGS(J1311).

References

- Bachmann, O., Bergantz, G.W., 2003. Rejuvenation of the Fish Canyon magma body: a window into the evolution of large-volume silicic magma systems. *Geology* 31, 789–792.
- Bachmann, O., Bergantz, G.W., 2004. On the origin of crystal-poor rhyolites: extracted from batholithic crystal mushes. *J. Petrol.* 45, 1565–1582.
- Bachmann, O., Dungan, M.A., Lipman, P.W., 2002. The Fish Canyon magma body, San Juan volcanic field, Colorado: rejuvenation and eruption of an upper-crustal batholith. *J. Petrol.* 43, 1469–1503.
- Barbarin, B., Didier, J., 1992. Genesis and evolution of mafic microgranular enclaves through various types of interaction between coexisting felsic and mafic magmas. *Earth Environ. Sci. Trans. R. Soc. Edinburgh* 83, 145–153.
- Barth, A., Feilen, A., Yager, S., Douglas, S., Wooden, J., Riggs, N., Walker, J., 2012. Petrogenetic connections between ash-flow tuffs and a granodioritic to granitic intrusive suite in the Sierra Nevada arc, California. *Geosphere* 8, 250–264.
- Barth, A., Wooden, J., Jacobson, C., Economos, R., 2013. Detrital zircon as a proxy for tracking the magmatic arc system: the California arc example. *Geology* 41, 223–226.
- Belousova, E., Griffin, W., O'Reilly, S.Y., 2006. Zircon crystal morphology, trace element signatures and Hf isotope composition as a tool for petrogenetic modelling: examples from eastern Australian granitoids. *J. Petrol.* 47, 329–353.
- Browne, B.L., Eichelberger, J.C., Patino, L.C., Vogel, T.A., Dehn, J., Uto, K., Hoshizumi, H., 2006. Generation of porphyritic and equigranular mafic enclaves during magma recharge events at Unzen Volcano, Japan. *J. Petrol.* 47, 301–328.
- Buret, Y., von Quadt, A., Heinrich, C., Selby, D., Wälle, M., Peytcheva, I., 2016. From a long-lived upper crustal magma chamber to rapid porphyry copper emplacement: Reading the geochemistry of zircon crystals at Bajo de la Alumbrera (NW Argentina). *Earth Planet. Sci. Lett.* 450, 120–131.
- Buret, Y., Wotzlaw, J.-F., Roozen, S., Guillong, M., von Quadt, A., Heinrich, C.A., 2017. Zircon petrochronological evidence for a plutonic-volcanic connection in porphyry copper deposits. *Geology* 45, 623–626.
- Cantagrel, J.-M., Didier, J., Gourgaud, A., 1984. Magma mixing: origin of intermediate rocks and “enclaves” from volcanism to plutonism. *Phys. Earth Planet. Inter.* 35, 63–76.
- Carley, T.L., Miller, C.F., Wooden, J.L., Padilla, A.J., Schmitt, A.K., Economos, R.C., Bindeman, I.N., Jordan, B.T., 2014. Iceland is not a magmatic analog for the Hadean: evidence from the zircon record. *Earth Planet. Sci. Lett.* 405, 85–97.
- Cashman, K.V., Sparks, R.S.J., Blundy, J.D., 2017. Vertically extensive and unstable magmatic systems: a unified view of igneous processes. *Science* 355, eaag3055.
- Chamberlain, K.J., Wilson, C.J., Wooden, J.L., Charlier, B.L., Ireland, T.R., 2014. New perspectives on the Bishop Tuff from zircon textures, ages and trace elements. *J. Petrol.* 55, 395–426.
- Claiborne, L.L., Miller, C., Walker, B., Wooden, J., Mazdab, F., Bea, F., 2006. Tracking magmatic processes through Zr/Hf ratios in rocks and Hf and Ti zoning in zircons: an example from the Spirit Mountain batholith, Nevada. *Mineral. Mag.* 70, 517–543.
- Claiborne, L.L., Miller, C.F., Wooden, J.L., 2010. Trace element composition of igneous zircon: a thermal and compositional record of the accumulation and evolution of a large silicic batholith, Spirit Mountain, Nevada. *Contrib. Mineral. Petrol.* 160, 511–531.
- Cooper, K.M., Kent, A.J., 2014. Rapid remobilization of magmatic crystals kept in cold storage. *Nature* 506, 480–483.
- Cooper, G.F., Wilson, C.J., Charlier, B.L., Wooden, J.L., Ireland, T.R., 2014. Temporal evolution and compositional signatures of two supervolcanic systems recorded in zircons from Mangakino volcanic centre, New Zealand. *Contrib. Mineral. Petrol.* 167, 1018.
- Deering, C., Bachmann, O., Dufek, J., Gravelly, D., 2011. Rift-related transition from andesite to rhyolite volcanism in the Taupo Volcanic Zone (New Zealand) controlled by crystal–melt dynamics in mush zones with variable mineral assemblages. *J. Petrol.* 52, 2243–2263.
- Deering, C.D., Keller, B., Schoene, B., Bachmann, O., Beane, R., Ovtcharova, M., 2016. Zircon record of the plutonic-volcanic connection and protracted rhyolite melt evolution. *Geology* 44, 267–270.
- Donaire, T., Pascual, E., Pin, C., Duthou, J.-L., 2005. Microgranular enclaves as evidence of rapid cooling in granitoid rocks: the case of the Los Pedroches granodiorite, Iberian Massif, Spain. *Contrib. Mineral. Petrol.* 149, 247–265.
- Ferry, J.M., Watson, E.B., 2007. New thermodynamic models and revised calibrations for the Ti-in-zircon and Zr-in-rutile thermometers. *Contrib. Mineral. Petrol.* 154, 429–437.
- Fohey-Breting, N., Barth, A., Wooden, J., Mazdab, F., Carter, C., Schermer, E., 2010. Relationship of voluminous ignimbrites to continental arc plutons: Petrology of Jurassic

- ignimbrites and contemporaneous plutons in southern California. *J. Volcanol. Geotherm. Res.* 189, 1–11.
- Gagnevin, D., Daly, J.S., Kronz, A., 2010. Zircon texture and chemical composition as a guide to magmatic processes and mixing in a granitic environment and coeval volcanic system. *Contrib. Mineral. Petrol.* 159, 579–596.
- Grimes, C., Wooden, J., Cheadle, M., John, B., 2015. "Fingerprinting" tectono-magmatic provenance using trace elements in igneous zircon. *Contrib. Mineral. Petrol.* 170 (46).
- Günther, T., Klemd, R., Zhang, X., Horn, I., Weyer, S., 2017. In-situ trace element and Fe-isotope studies on magnetite of the volcanic-hosted Zhibo and Chagangnuoer iron ore deposits in the Western Tianshan, NWChina. *Chem. Geol.* 453, 111–127.
- He, Z.Y., Xu, X.S., 2012. Petrogenesis of the Late Yanshanian mantle-derived intrusions in southeastern China: response to the geodynamics of paleo-Pacific plate subduction. *Chem. Geol.* 328, 208–221.
- He, Z., Xu, X., Yu, Y., Zou, H., 2009. Origin of the Late Cretaceous syenite from Yandangshan, SEChina, constrained by zircon U-Pb and Hf isotopes and geochemical data. *Int. Geol. Rev.* 51, 556–582.
- Hildreth, W., 2004. Volcanological perspectives on Long Valley, Mammoth Mountain, and Mono Craters: several contiguous but discrete systems. *J. Volcanol. Geotherm. Res.* 136, 169–198.
- Hoskin, P.W., Schaltegger, U., 2003. The composition of zircon and igneous and metamorphic petrogenesis. *Rev. Mineral. Geochem.* 53, 27–62.
- Jahn, B.M., 1974. Mesozoic thermal events in Southeast China. *Nature* 248, 480–483.
- Kemp, A.I.S., Hawkesworth, C.J., Foster, G.L., Paterson, B.A., Woodhead, J.D., Hergt, J.M., Gray, C.M., Whitehouse, M.J., 2007. Magmatic and crustal differentiation history of granitic rocks from Hf-O isotopes in zircon. *Science* 315, 980–983.
- Kennedy, B., Stix, J., Hon, K., Deering, C., Gelman, S., 2016. Magma storage, differentiation, and interaction at Lake City caldera, Colorado, USA. *Bulletin* 128, 764–776.
- Kirkland, C.L., Smithies, R.H., Taylor, R.J.M., Evans, N., McDonald, B., 2015. Zircon Th/U ratios in magmatic environs. *Lithos* 212–215, 397–414.
- Klemetti, E.W., Deering, C.D., Cooper, K.M., Roeske, S.M., 2011. Magmatic perturbations in the Okataina Volcanic Complex, New Zealand at thousand-year timescales recorded in single zircon crystals. *Earth Planet. Sci. Lett.* 305, 185–194.
- Large, S.J., Quadt, A.v., Wotzlaw, J.-F., Guillong, M., Heinrich, C.A., 2018. Magma evolution leading to porphyry Au-Cu mineralization at the Ok Tedi deposit, Papua New Guinea: Trace element geochemistry and high-precision geochronology of igneous zircon. *Econ. Geol.* 113, 39–61.
- Perugini, D., Poli, G., 2012. The mixing of magmas in plutonic and volcanic environments: analogies and differences. *Lithos* 153, 261–277.
- Reid, M.R., Vazquez, J.A., Schmitt, A.K., 2011. Zircon-scale insights into the history of a Supervolcano, Bishop Tuff, Long Valley, California, with implications for the Ti-in-zircon geothermometer. *Contrib. Mineral. Petrol.* 161, 293–311.
- Schmitt, A.K., Klitzke, M., Gerdes, A., Schäfer, C., 2017. Zircon Hafnium–Oxygen isotope and trace element petrochronology of intraplate volcanic rocks from the Eifel (Germany) and implications for mantle versus crustal origins of zircon megacrysts. *J. Petrol.* 58, 1841–1870.
- Shellnutt, J., Jahn, B.-M., Dostal, J., 2010. Elemental and Sr–Nd isotope geochemistry of microgranular enclaves from peralkaline A-type granitic plutons of the Emeishan large igneous province, SWChina. *Lithos* 119, 34–46.
- Stelten, M.E., Cooper, K.M., Vazquez, J.A., Calvert, A.T., Glessner, J.J., 2015. Mechanisms and timescales of generating eruptible rhyolitic magmas at Yellowstone caldera from zircon and sanidine geochronology and geochemistry. *J. Petrol.* 56, 1607–1642.
- Storm, S., Schmitt, A.K., Shane, P., Lindsay, J.M., 2014. Zircon trace element chemistry at sub-micrometer resolution for Tarawera volcano, New Zealand, and implications for rhyolite magma evolution. *Contrib. Mineral. Petrol.* 167, 1000.
- Vernon, R., 1984. Microgranitoid enclaves in granites–globules of hybrid magma quenched in a plutonic environment. *Nature* 309, 438–439.
- Wang, D.Z., Zhou, J.C., Qiu, J.S., Fan, H.H., 2000. Characteristics and petrogenesis of Late Mesozoic granitic volcanic–intrusive complexes in Southeastern China. *Geol. J. China Univ.* 6, 487–498 (in Chinese with English abstract).
- Wark, D.A., Miller, C.F., 1993. Accessory mineral behavior during differentiation of a granite suite: monazite, xenotime and zircon in the Sweetwater Wash pluton, southeastern California, U.S.A. *Chem. Geol.* 110, 49–67.
- Wotzlaw, J.-F., Schaltegger, U., Frick, D.A., Dungan, M.A., Gerdes, A., Günther, D., 2013. Tracking the evolution of large-volume silicic magma reservoirs from assembly to supereruption. *Geology* 41, 867–870.
- Wright, H.M., Folkes, C.B., Cas, R.A., Cashman, K.V., 2011. Heterogeneous pumice populations in the 2.08-Ma Cerro Galán Ignimbrite: implications for magma recharge and ascent preceding a large-volume silicic eruption. *Bull. Volcanol.* 73, 1513–1533.
- Yan, L.-L., He, Z.-Y., Jahn, B.-m., Zhao, Z.-D., 2016. Formation of the Yandangshan volcanic–plutonic complex (SE China) by melt extraction and crystal accumulation. *Lithos* 266–267, 287–308.
- Yan, L., He, Z., Beier, C., Klemd, R., 2018. Geochemical constraints on the link between volcanism and plutonism at the Yunshan caldera complex, SEChina. *Contrib. Mineral. Petrol.* 173, 4.
- Zhou, X.M., Sun, T., Shen, W.Z., Shu, L.S., Niu, Y.L., 2006. Petrogenesis of Mesozoic granitoids and volcanic rocks in South China: a response to tectonic evolution. *Episodes* 29, 26–33.